Design of optimal multi-site brain stimulation protocols via neuro-inspired epilepsy models for abatement of interictal discharges

Marouan Arrais, Julien Modolo, David Mogul, Fabrice Wendling

Design of optimal multi-site brain stimulation protocols via neuro-inspired epilepsy models for abatement of interictal discharges

Marouan Arrais[1], Julien Modolo[1,*], David Mogul[2], Fabrice Wendling[1]

[1]Univ Rennes, INSERM, LTSI – U1099, F-35000 Rennes, France.

[2]Department of Biomedical Engineering, Illinois Institute of Technology, Chicago, USA.

***Corresponding author:** julien.modolo@inserm.fr, Laboratoire Traitement du Signal et de l'Image (LTSI), Bâtiment 22 Campus de Beaulieu, 35042 Rennes Cedex, France.

Abstract

Background. Electrical brain stimulation is recognized as a promising therapeutic approach for treating brain disorders such as epilepsy. However, the use of this technique is still largely empirical, since stimulation parameters and targets are chosen using a trial-and-error approach. Therefore, there is a pressing need to design optimal, rationale-based multi-site brain stimulation protocols to control epileptiform activity. **Approach**. Here, we developed biologically-inspired models of brain activity receiving stimulation at two levels of description (single- and multi-population epileptogenic networks). First, we used bifurcation analysis to determine optimal parameters able to abort epileptiform patterns. Second, we present a graph-theory based method to classify network populations in an epileptogenic network based on their contribution to seizure generation and propagation. **Main results**. The best therapeutic effects (i.e., reduction of epileptiform discharges duration and occurence rate) were obtained by the specific targeting of populations with the highest eigenvector centrality values. The timing of stimulation was also found to be critical in seizure abortion impact. **Significance**. Overall, our results provide a proof-of-concept that using network neuroscience combined with physiology-based computational models of brain activity can provide an effective method for the rational design of brain stimulation protocols in epilepsy.

Keywords: epilepsy, brain stimulation, computational modeling, dynamical systems, neural mass model.

1 Introduction

Epilepsy is one of the most prevalent neurological disorders, affecting more than seventy million people worldwide (approx. 1% of the world population) (Katchanov and Birbeck, 2012; Ngugi et al., 2011). It is characterized by recurrent seizures (Kwan and Brodie, 2000) that dramatically impair patients' quality of life. Seizures are primarily

related to excessive and synchronized neural discharges in one or several brain structures (Badawy et al., 2012). The most immediate therapy for treating and controlling epilepsy is the use of drugs, or possibly a combination of drugs (Sankaraneni and Lachhwani, 2015). However, one third of epileptic patients do not respond to drug therapy (Kobau et al., 2008). Surgery can be an option for those patients, however, a large fraction of patients (60-70%) is not eligible due to an unfavorable benefit/risk ratio. Consequently, there is a pressing need for alternative therapies that could significantly decrease seizure frequency. Among candidate approaches, brain stimulation is receiving increasing attention by the research community.

It has been indeed demonstrated decades ago (Upton and Cooper, 1976) that electrical brain stimulation can alter epileptiform activity, motivating research efforts to identify its mechanisms of action and optimize its therapeutic effects. Moreover, several fMRI, MEG and EEG studies have revealed the existence of brain regions having denser connections than others (Lee et al., 2018; Youssofzadeh et al., 2018) eliciting and encouraging investigation of multisite stimulation. Accordingly, experimental studies have recognized a link between an improvement in the effectiveness of brain stimulation in terminating epileptic seizures and the choice of stimulation populations where multi-site stimulation is applied (Sobayo and Mogul, 2016). However, the clinical use of brain stimulation in the context of epilepsy is still limited and largely based on a trial-and-error approach (Hoang et al., 2017). Besides, the studies focusing on parameters (intensity, frequency, waveform, …) are still few, mostly empirical and based on qualitative assessments. This problem is due to the fact that the accurate characterization of the stimulation response at bedside cannot be achieved, since this would require extensive sessions which are not compatible with patients' limited time and tolerance. An alternative approach is to perform animal *in vivo* and *in vitro* experiments to identify the most effective parameters, which may not be a practical approach since the entire stimulation parameter space is too large to be practical to explore.

In this context, one possibility to identify optimal stimulation parameters, while avoiding such unrealistic extended testing sessions of stimulation parameters, consists in using neuro-inspired computational models. Over the past decades, such models have been developed to simulate brain activity at different spatiotemporal scales. Microscopic models (Hodgkin and Huxley, 1952) describe single neuron dynamics, while mesoscopic models, such as neural mass models (NMMs) (Jansen and Rit, 1995; Wendling et al., 2002) or neural field models (Spiegler and Jirsa, 2013) describe the average activity of neuronal assemblies. In the field of epilepsy, computational models have gained acceptance and are now recognized as an efficient approach to get insights into the pathophysiological mechanisms underlying epileptiform activity (Wendling et al., 2016). Among these models, the choice of NMMs to model epileptiform activity is motivated by their ease of use (small number of parameters as compared to microscopic models), while retaining key neuroanatomical and neurophysiological properties. Furthermore, NMMs enable simulating signals at the same scale as electrophysiological signals typically recorded in clinics, from scalp

(EEG) or intracerebral (depth-EEG, SEEG, or ECoG) signals. One pioneering NMM model is the Jansen and Rit model (Jansen and Rit, 1995), initially developed to study visual evoked potentials, later adapted to generate epileptiform activities under appropriate values of excitation- and inhibition-related parameters (Wendling et al., 2000).

In this paper, we modeled functionally connected epileptogenic regions by coupling modified Jansen and Rit NMMs, enabling the study of network effects in response to stimulation-like perturbations. We used this approach to determine relevant regions driving and controlling epileptiform activity. In addition, we compared single-site with multi-site stimulation, and designed optimal strategies to restore desynchronized neuronal activities and abort global epileptiform activity at the network scale. The paper is organized as follows. Section 2 presents the modified Jansen and Rit NMM, the constructed network and the index used to quantify stimulation efficiency. Then, in Section 3 we analyze stimulation effects on a single region and determine optimal stimulation parameters using a mathematical approach derived from control theory and bifurcation analysis. We also investigate how subpopulations contribute to seizure termination and the resonance phenomena. These results are then used as the basis to study multi-site stimulation effects on a complete network involving seven regions. We study the impact of the spatial distribution of a potentially effective electrical stimulation on neuronal activity, and also show how stimulation targets could be chosen from patient electrophysiological signals. Results reveal the superiority of multi-site stimulation as compared to single-site stimulation, and indicate that stimulating regions with the largest number of outgoing connections, as estimated using a graph theory metric, is the most efficient. Finally, we examine the impact of the stimulation timing and strategies (closed- vs open-loop) on epileptiform activity control efficacy.

2 Materials and Methods

2.1 Modeling epileptogenic networks of coupled neuronal populations accounting for stimulation

The Jansen and Rit model describes the activity of a neuronal population composed of two subsets of neurons: excitatory glutamatergic cells (i.e. pyramidal cells) and inhibitory GABAergic interneurons. Each subset is described by two functions; the first one is the “pulse-to-wave” function, $h_e(t)$ or $h_i(t)$, converting the density of presynaptic action potentials into an average excitatory (EPSP) or inhibitory (IPSP) post synaptic potential. This function acts as a linear second-order low-pass filter and includes physiological time constants. The second one is the “wave-to-pulse” function, converting incoming post synaptic potentials into a population firing rate. This static function was proposed by Freeman (Freeman, 1975):

$$Sig(v) = \frac{v_{max}}{2}\left(1 + tanh\ \frac{r}{2}(v - v_0)\right) = \frac{v_{max}}{1 + e^{r(v_0 - v)}} \quad \textbf{(1)}$$

where v_{max} is the maximum firing rate, v_0 the value of the average membrane potential acting as a firing threshold, and r the slope of the sigmoid at v_0. In the model, interactions between pyramidal cells and interneurons are represented by four connectivity constants, C_1 to C_4 representing the average number of synaptic contacts. The model is summarized below in Figure 1a) and 1b).

Here, we modified the original Jansen and Rit model by adding a stimulation term denoted in the following by "Stim" as an additional input to sigmoid functions (Suffczynski et al., 2008). Here, the assumption is that the electric field generated by electrical stimulation has a direct de- or hyper-polarization linear effect onto the mean membrane potential of neuron subsets (Radman et al., 2009). This model extension leads to the following set of differential equations:

$$\begin{aligned}
\dot{y}_0(t) &= y_3(t) \\
\dot{y}_3(t) &= AaSig(k_e Stim(t) + y_1(t) - y_2(t)) - 2ay_3(t) - a^2 y_0(t) \\
\dot{y}_1(t) &= y_4(t) \\
\dot{y}_4(t) &= Aa\{p(t) + C_2 Sig(k_e Stim(t) + C_1 y_0(t))\} - 2ay_4(t) - a^2 y_1(t) \\
\dot{y}_2(t) &= y_5(t) \\
\dot{y}_5(t) &= BbC_4 Sig(k_i Stim(t) + C_3 y_0(t)) - 2by_5(t) - b^2 y_2(t)
\end{aligned} \qquad \textbf{(2)}$$

where A and B denote the amplitude of average EPSPs and IPSPs, respectively; where a and b (expressed in s^{-1}) represent physiological time constants. The local field potential (LFP) reflecting the population activity is expressed by the term $y_1(t) - y_2(t)$, representing the summation of excitatory postsynaptic excitatory and inhibitory potentials onto pyramidal cells. In order to study the impact of selectively targeting neuronal subpopulations, for example excitatory (e) pyramidal cells and inhibitory (i) interneurons, the stimulation magnitude is multiplied by two coefficients k_e and k_i respectively, chosen as follows: $(k_e, k_i) \in \{(1,1),(1,0),(0,1)\}$ $(figure\ 1b)$. The values and physiological meaning of model parameters are provided in Table 1.

Parameter	Description	Value
A, B	Averages of excitatory and inhibitory synaptic gains, respectively.	$A = 3.85\ mV$ $B = 15\ mV$
a, b	Average time constants of postsynaptic potentials.	$a = 100\ s^{-1}$ $b = 30\ s^{-1}$
C_1, C_2, C_3, C_4	Average number of synaptic contacts of excitatory and inhibitory connections.	$C_1 = J$ $C_2 = 0.8 \times J$ $C_3 = 0.25 \times J$ $C_4 = 0.25 \times J$ where $J = 135$

v_0, v_{max}, r	Threshold, maximum output, and slope of the sigmoid function $Sig(v)$.	$v_0 = 6\ mV$ $v_{max} = 5\ s^{-1}$ $r = 0.56\ mV^{-1}$

Table 1. Physiological meaning and values of the parameter values of a single Jansen and Rit model.

Network architecture. As presented in Figure 1c, the network consisted in seven populations denoted by $NM_i, i \in \{1, \dots, 7\}$. Each region was modelled using the modified Jansen and Rit NMM presented below (Figure 1d). The parameter values were equal to those in Table 1 except the inhibitory synaptic gain that was changed to 16.7 mV to ensure and maintain the generation of interictal discharges. Interictal discharges are recognized as biomarkers of epileptic seizures (Roehri et al., 2018). These interictal oscillations mirror specific, dynamic changes in neuronal excitability causing ictogenesis. Therefore, they play a precipitating role in seizure occurrence and are also used to localize epilepsy focus (Lévesque et al., 2018). White Gaussian noise was added to the firing rate of incoming excitatory input onto pyramidal cells in each NMM, with a mean m and a standard deviation σ equal to 90 Hz and 1.2, respectively. We used the Euler-Maruyama method to solve the set of equations (Maruyama, 1955). The network was fully connected, in that each NMM received afferents from all other NMMs; action potentials of pyramidal cells of all $NM_j, j \in \{1, \dots, 7\}, j \neq i$ were added at the level of pyramidal cells of NM_i (Figure 1d). These afferents were modulated through a NMM-dependent connectivity constants $C_{i,j}, i, j \in \{1, \dots, 7\}$and a propagation delay arbitrarily chosen as 30 ms. The connectivity matrix was a hollow matrix with dimensionless components chosen uniformly within the interval [0, 1.7]. Those randomly chosen values were kept fixed for all simulations.

Stimulation. Stimulation waveform is another key parameter in determining the impact of neuromodulation on brain tissue. We used a square bi-phasic waveform to mimic the charge-balanced biphasic pulse stimulation commonly used in practice (figure 1-c). Compared to monophasic pulse stimulation or direct current stimulation, bi-phasic stimulation limits irreversible damage caused by charge accumulation in the tissue. The stimulation of network populations was altered *via* population-dependent coupling coefficients $k_i \in \{0, 1\}, \forall\, i \in \{1, \dots, 7\}$, as presented in Figure 2c.

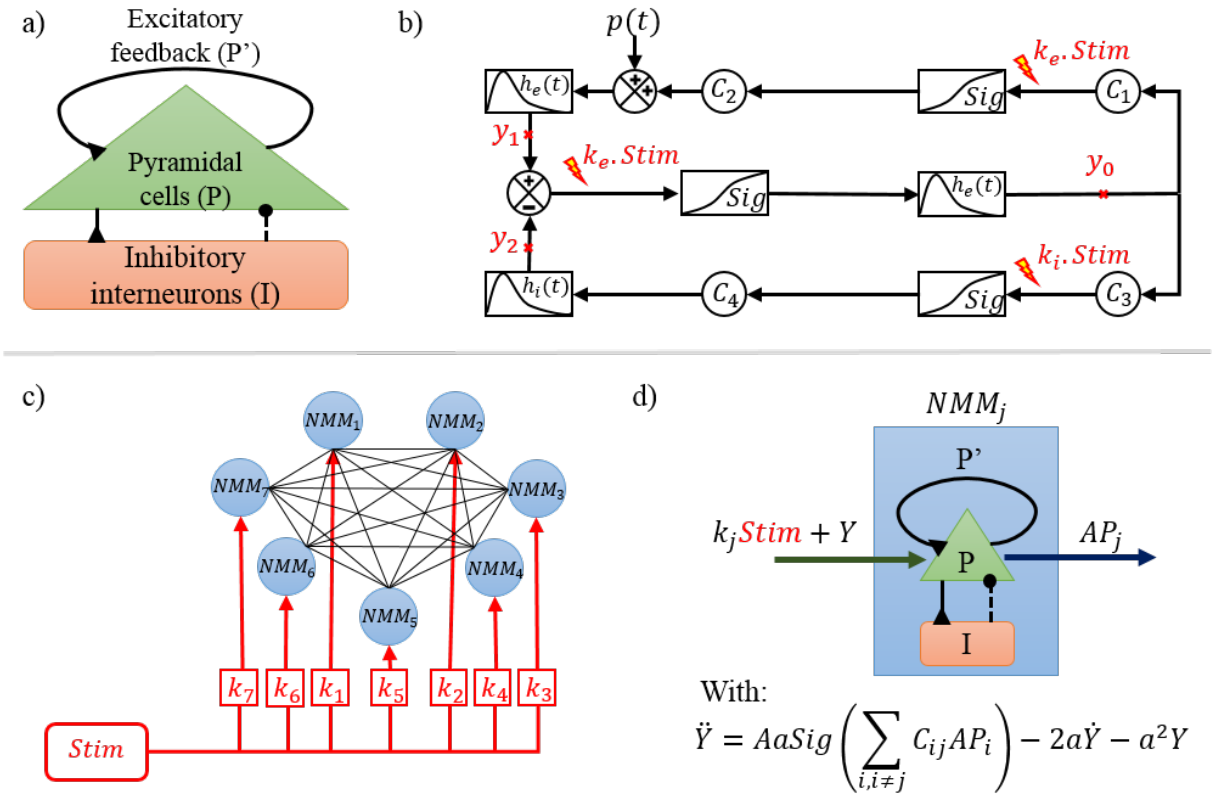

Figure 1. a) Structure and b) Block diagram of the modified Jansen and Rit NMM accounting for stimulation. c) Diagram of the complete network allowing for single-site and multi-site stimulation, and d) block diagram of each node with its input and output. a) Population of pyramidal cells (green triangle) interacts with an inhibitory population of interneurons (orange rectangle). Solid-lines arrows represent excitatory connections, while dashed-lines represent inhibitory ones. b) $y_i\,(t)\,, i \in \{0, 1, 2\}$ correspond to the output of pyramidal cells, excitatory and inhibitory interneurons, respectively. $p(t)$ is a white Gaussian noise representing excitatory inputs from neighboring areas. The "Stim" symbol represents a modification with respect as compared to the original Jansen and Rit model, where electrical stimulation is applied in the model depending on coefficients $k_e$and k_i. c and d) The network is composed of 7 fully connected NMMs. Each node receives stimulation (bi-phasic waveform) with population-dependent coupling coefficients $k_i, i \in \{1, \ldots, 7\}$, in addition to afferents from other NMMs. The afferents received by a given NMM *j* from a given NMM *i* with $i \in \{1, \ldots, 7\}$and $i \neq j$ are converted into a postsynaptic potential before being added as an input to pyramidal cells. The $C_{i,j}, i, j \in \{1, \ldots, 7\}$ coefficients represent connectivity constants between network populations.

2.2 Quantification of stimulation efficiency

In order to quantify the efficiency of stimulation for suppressing epileptic discharges, we devised a new index based on their occurrence. It is referred to as the amount of epileptic discharges index (*AEDI*) and defined as follows:

$$AEDI = \sum_i N_i \Delta_i^4 \quad \textbf{(3)}$$

where N_i represents the number of occurrences of an interval of a duration $\Delta_i$during which epileptic activity is observed. The duration exponent emphasizes the duration of interictal discharges. This index quantifies the number and duration of time intervals exhibiting epileptic discharges. Every stimulation protocol leading to the reduction of *AEDI* versus the AEDI computed without stimulation (control condition) is considered to have a therapeutic effect. The issue is to identify stimulation parameters (amplitude, frequency, populations to stimulate) which maximize this reduction (i.e. minimize *AEDI*). In practice, therapeutic effect is marked by an increase/decrease of short/long Δ_i on the histogram.

Thus, once a stimulation was delivered, we summend the absolute values of the signals of all 7 populations composing the network. The obtained signal was then processed to discriminate the intervals exhibiting epileptic activity from those with background activity. For this purpose, we started by applying a linear filter twice, once forward and once backwards, using the already implemented filtfilt function in Python's Scipy library. By using this filter, we limited fluctuations and obtained a smoother signal. Then, we defined a signal amplitude-dependent threshold for differentiation. The intervals exhibiting background activity were ignored, while others were quantified with respect to their duration (example in Figure 3c and 3d). Histograms showing their occurrence with respect to their duration were generated and AEDI values were computed.

2.3 Optimal stimulation: how many populations and which ones?

We studied the efficiency of stimulation as a function of the number of populations stimulated for 1000 neuronal networks, each composed of 7 fully connected NMMs. These constructed networks had the same parameter values (synaptic gains, time constants, synaptic contacts), and what differed between those networks were the connectivity coefficients ($k_n, n \in \{1, \dots, 7\}$) and the excitatory noise entering each neuronal population which were randomly generated. The noise describing the influence of neighboring NMMs was a white Gaussian noise of mean and standard deviation equal to (90, 1.2), while the connectivity coefficients were randomly chosen. For each network, we stimulated following all the possible stimulation combinations of variables $(k_1, \dots, k_7)$. The stimulation could be applied following 127 different ways. This number represents all the possible combinations that could be obtained for the set $\{(k_1, \dots, k_7), \forall k_n \in \{0, 1\}, n \in \{1, \dots, 7\}\}$ minus the case were all the coupling $(k_1, \dots, k_7) = (0, \dots, 0)$, where no stimulation is applied. A total of 127000 simulations were performed and the corresponding AEDI values were computed.

To classify network populations according to their impact on the whole network activity, we used a graph theory measure known as eigenvector centrality (EVC), which

was used to score the influence of each node. Computed on functional connectivity matrices, a high EVC value means that a considered node is connected to have preferential connections to other populations in the network and drives their activity. In practice, we made use of LFPs. To determine connectivity matrices, we computed the degree of coupling between network populations, while considering the directionality of coupling. Connectivity matrices were computed from the nonlinear correlation coefficient h^2 (Lopes da Silva et al., 1989; Pijn and Lopes da Silva, 1993) which is given by:

$$h^2 = \frac{\sum_{i=1}^{N}\left(y_i - \underline{y}\right)^2 - \sum_{i=1}^{N}\left(y_i - f(x_i)\right)^2}{\sum_{i=1}^{N}\left(y_i - \underline{y}\right)^2} \quad \textbf{(4)}$$

Where $y_i, x_i, \forall i \in [1, N]$ represent samples of two LFP signals generated by two populations x, y. f is a piecewise function passing from midpoints $(\underline{x}, \underline{y})$ after presenting the amplitude signal y with respect to that of signal x and dividing the x-axis into equal sized bins. These linear line segments form a linear approximation of the nonlinear regression curve. The correlation value varies between 0 (no association between signals) and 1 (one signal is fully predictable based on the other).

Finally, results were compared to ground-truth connectivity matrices explicitly known for each network model.

3 Results

3.1 Impact of stimulation parameters in a single NMM

We tuned the synaptic gains (Table 1) of the NMM to generate interictal discharges, as shown in Figure 2a. We then evaluated the impact of sinusoidal stimulation parameters (amplitude, frequency) on the neuronal population activity. Results are summarized in the bifurcation diagram of Figure 2, which shows the changes of dynamics under the stimulation perturbation.

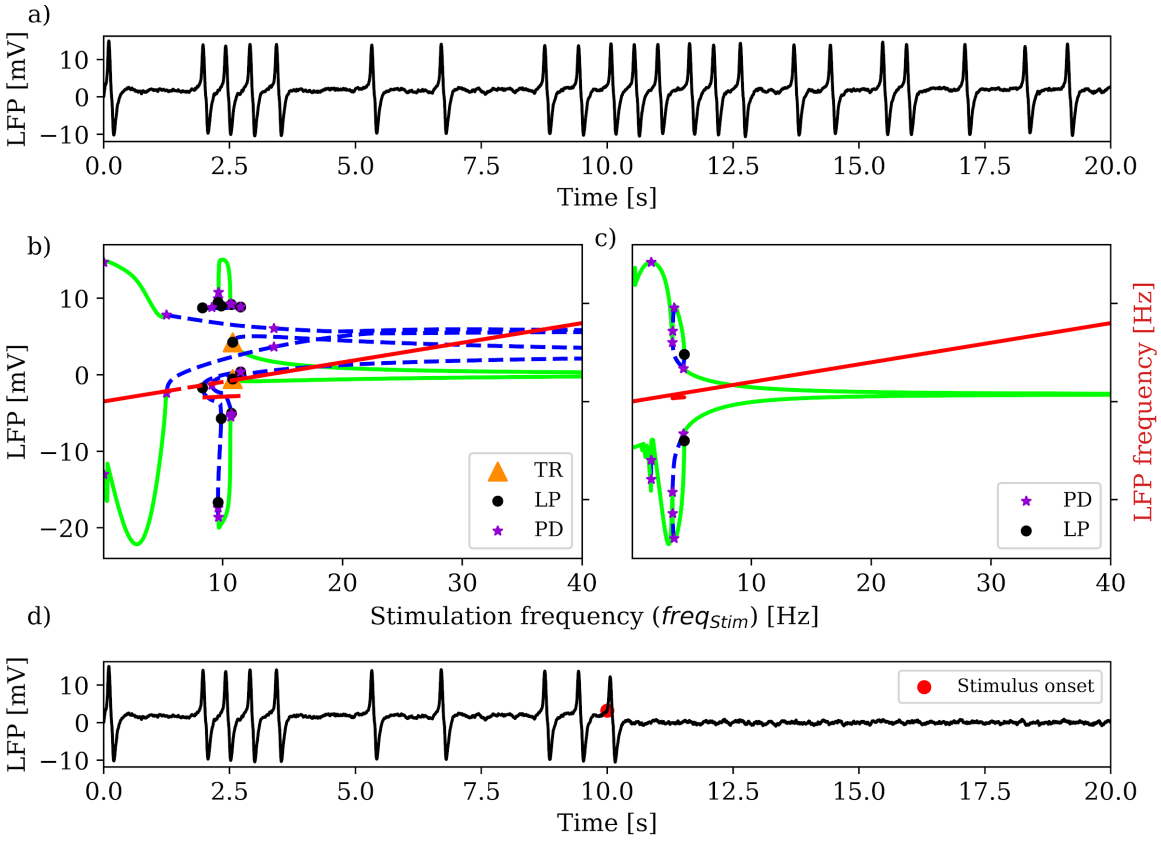

Figure 2. Analysis of effects of stimulation on a single NMM (single population).

a) Simulated interictal discharges under no stimulation condition. b) Sinusoidal stimulation (amplitude 3 mV, frequency ranging from 0 to 150 Hz) applied to all neuronal subpopulations. For the sake of readability, results are shown for stimulation frequencies within the [0, 40] Hz range. c) Sinusoidal stimulation (amplitude 3 mV, frequency ranging from 0 to 150 Hz) applied only to inhibitory interneurons. b,c) In both cases system dynamics depend on stimulation parameters as depicted by LFP amplitudes (blue and green curves) and frequencies (red curves). Stable and unstable limit cycles are represented by solid green and dashed blue lines, while their frequencies are represented by solid and dashed red lines, respectively. Abbreviations; LP: fixed point, PD: period doubling, TR: Torus attractor. d) LFP signal observed for optimal stimulation parameters (amplitude 3 mV, frequency 90 Hz). To generate sporadic discharges, average excitatory (A) and inhibitory (B) synaptic gains were fixed at 3.85 mV and 15 mV, respectively.

Figure 2-b,c illustrates all the dynamics that system (2) can generate while varying the frequency of a sinusoidal stimulation applied either on all neuronal subpopulations (Figure 2-b), or only to inhibitory interneurons (Figure 2-c). It is then possible to distinguish between stimulation frequencies for which the system generates high-amplitude oscillations, and those for which the system is attracted to a small, stable limit cycle that can be considered as a stable limit point. In addition, it highlights the sensitivity to neurostimulation parameters and reveals the effects of neuronal selectivity.

The bifurcation diagram presented in Figure 2-b can be divided into three regions. In the first region where $freq_{Stim} \in [0, 5.18[$, the system is attracted by stable limit cycles and generates rhythmic activities of increasing frequencies and modulated amplitudes. In the second region where $freq_{Stim} \in [5.18, 10.83[$Hz, the population activity is altered and unsteady. We detect closed trajectories of limit cycles with different amplitude ranges and numerous period doublings where oscillations of double the period of original ones are induced. Throughout this interval, the LFP is of an oscillatory activity involving a mix of frequencies and amplitudes. Third, for $freq_{Stim} \in [10.83, 150]$Hz, we detect a saddle-node bifurcation for periodic orbits coupled to a subcritical Neimark-Sacker bifurcation for $freq_{Stim} = 10.83$ Hz. Beyond these bifurcation points, a pair of limit cycles, stable and unstable (solid-green and dashed-blue lines), are created and the system is attracted by stable limit cycles of decreasing amplitudes. Increasing stimulation frequency (typically > 50 Hz) leads to periodic oscillations of frequency identical to the stimulation frequency, and of amplitude close to zero.

The bifurcation diagram presented in Figure 2-c exhibits similar dynamics, since global activity is still altered until reaching a separation stimulation frequency from which the amplitude of the oscillating activity decreases. Interestingly, unstable cycles (dashed blue lines) disappear while stimulating only inhibitory interneurons. This highlights the differential effects of stimulation depending on specific neuronal subtypes that are targeted and impacted. We observe that the stimulation frequency required to abort epileptiform activity is lower when stimulating GABAergic interneurons when compared to all subpopulations.

Those results provide a first indication of the potential parameters able to locally abort epileptiform activity, and replace it by an electrophysiological pattern closer to physiological activity (Figure 2d). In the next section, we take advantage of the knowledge at the single population level to attempt controlling epileptic activity in extended networks of neuronal populations.

3.2 Network model: single-site *versus* multi-site stimulation

From the single-site stimulation study, we retained the following stimulation parameters for multi-site stimulation: amplitude equal to 3 mV and a frequency equal to 90 Hz. In order to mimic stimulation protocols routinely performed in clinical epileptology, biphasic pulse stimulation was preferred to sinusoidal stimulation. Pulse stimulation (amp=3mV, $freq_{Stim}$=90 Hz, pulse width=5 ms per phase) was delivered on pyramidal cells and interneurons subpopulations as soon as epileptic spiking activity was detected in one node of the network. Stimulation duration was set to 1s, and was delivered only during time intervals showing epileptic activity for more than 1s. Spiking periods of shorter durations were not considered (no stimulation delivered).

In simulated networks, populations were represented by NMMs in which parameters were set to generate interictal spikes. In the presence of connections, these epileptic spikes showed higher degree of synchronization as depicted in the example of Figure 3a for a network of 7 populations.

Epochs of epileptic activity and background activity are reflected in Figure 3b as summation Σ of individual LFPs generated at each node and shown in Figure 3a.

Therefore, Σ was used to determine multi-site stimulation onset times. As depicted in Figure 3b, stimulation times (red dots) could be correctly determined, i.e. as soon as at least one node of the network generated epileptiform activity.

Figure 3c presents the impact of stimulation delivered at these stimulation times when one node was stimulated, while Figure 3d shows this impact when stimulation was applied simultaneously on all populations at the exact same times. Interestingly, multi-site stimulation leads to shorter epochs of epileptic activity and longer epochs of background activity.

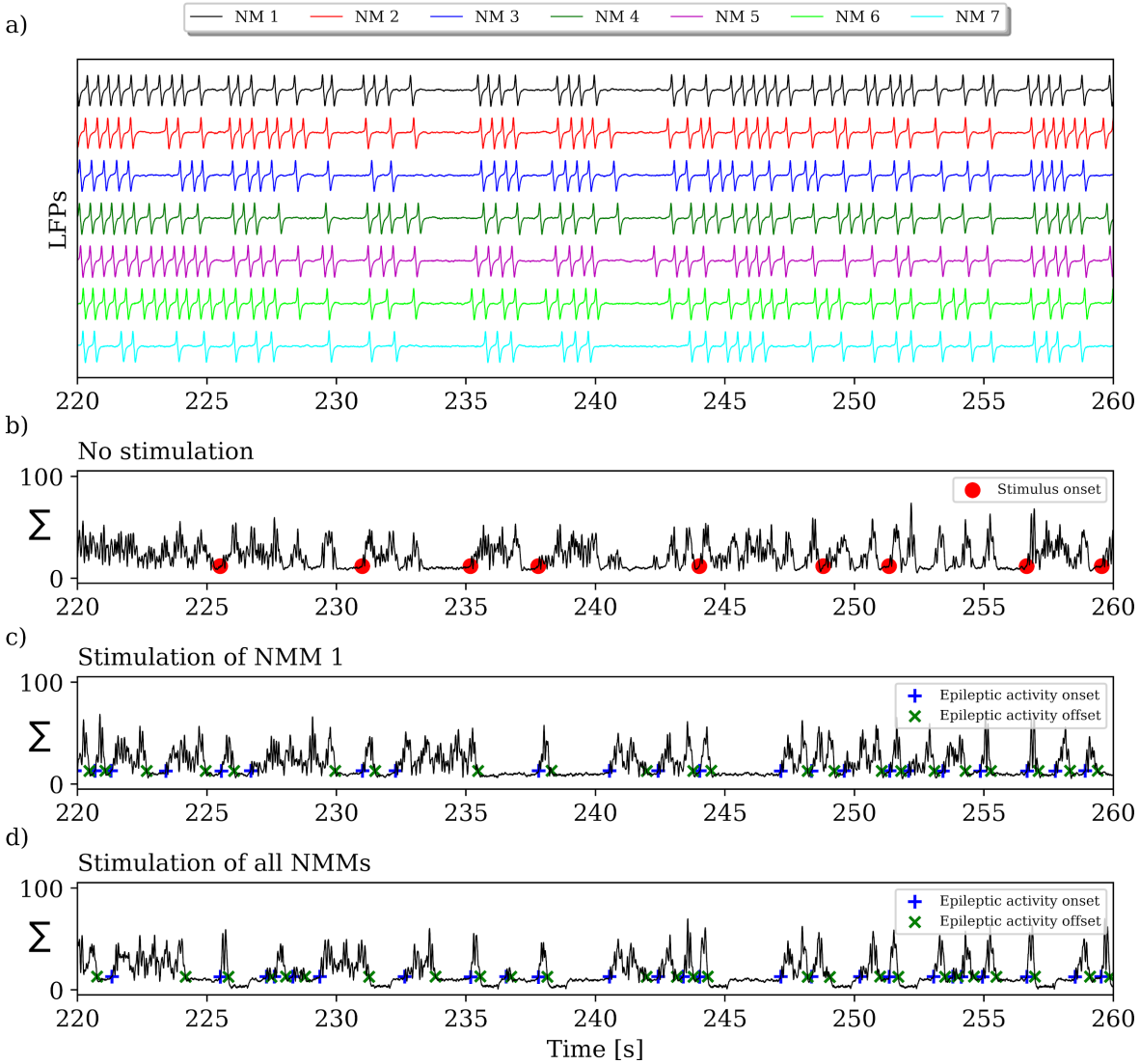

Figure 3. a) Individual LFPs of each NMM belonging to the network in the absence of electrical stimulation, and b) their summation. c, d) LFP summation after applying a charge-balanced (biphasic) stimulation of amplitude, frequency and pulse width of 3 mV, 90 Hz and 5 ms, on NMM 1 in (c) and all NMMs in (d); respectively. The duration of the stimulus was set to 1s. Red circles indicate stimulus

onsets, while blue and green markers indicate respectively the beginning and end of epileptic activity.

Using Σ, we first determined the number of populations to stimulate to obtain the highest therapeutic effect as denoted by minimal AEDI values. To proceed, we first evaluated the stimulation impact on the network using Σ as a function of the number of NMMs stimulated. For this purpose, we simulated LFPs while applying all the 127 possible combinations for the stimulation and compared *AEDI*s (number and choice of populations to stimulate). Then, we focused on how to identify the optimal NMM to be stimulated from LFP signals. In our investigation, we used the nonlinear correlation coefficient h^2, presented in the Methods section, to estimate connectivity links between network NMMs, and computed EVC values to determine the stimulation targets. Ground truth connectivity matrices were used to validate model-based predictions.

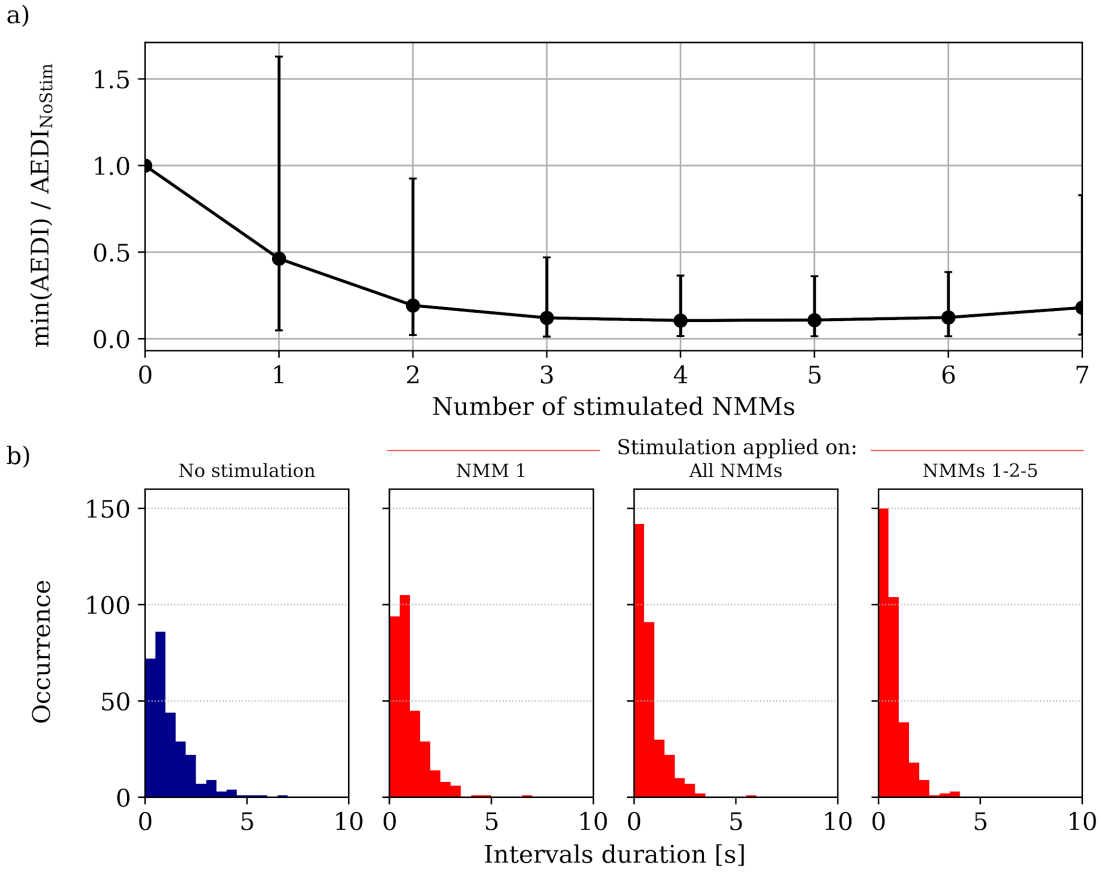

Figure 4. a) Normalized *AEDI* as a function of the number of stimulated NMMs in the network. b) Histograms of epileptic discharges occurrence with respect to their duration. The same charge-balanced biphasic stimulation (amplitude 3 mV, frequency 90 Hz, pulse width 5 ms) was used for all simulations.

Figure 4 confirms the effectiveness of multi-site stimulation as compared to single-site stimulation. Furthermore, it shows that stimulating a network subset is sufficient and efficient, in terms of *AEDI*, than stimulating the whole network (optimal situation -

minimal normalized AEDI when we stimulate four NMMs - see Figure 4a). For each network simulation, 127 stimulation possibilities were tested, and the minimal *AEDI* obtained while stimulating the same number of NMMs was retained, and an average value over all simulations was plotted. We identified the optimal number of NMMs to stimulate as equal to four. However, starting from 3 and up to 6 NMMs, the difference in *AEDI*s was minimal.

Targeted network populations. For each simulation of the 1000 simulations performed to study the efficiency of stimulation with respect to the number of stimulated populations, we computed the nonlinear correlation between LFPs of the network. Then, EVC was used to score the influence of population on others. Higher scores point out populations possessing a higher number of outgoing connections. Results were compared to ground-truth connectivity matrices used to construct the networks. Interestingly, EVC values predicted correctly 2 out of 3 optimal stimulation targets 862 times (89.2% of simulations), the exact same three NMMs 375 times (38.8%), and at least two NMMs 487 times (50.4%).

Regarding the simulation presented in Figure 3a, the reconstructed connectivity matrix identified NMMs 1, 2 and 5 as those most involved in epileptiform activity propagation. Interestingly, the same NMMs were detected by the calculation of the eigenvector centrality suggesting that the level of induced network synchrony was a key factor in stimulation efficacy (Good et al., 2009). While testing all 35 (=7! / (3!×4!)) possible combinations for targeting 3 NMMs out of 7 NMMs, the minimal normalized AEDI was equal to 0.15. This AEDI value was lower than the one when all 7 NMMs were stimulated. Figure 4b presents the resulting histograms in the absence of stimulation and while stimulating NMM 1, the whole network, and the set {NMM1, NMM2, NMM5}, respectively.

3.3 Stimulation strategy: open- *versus* closed-loop and impact of stimulation timing with respect to epileptic discharge onset

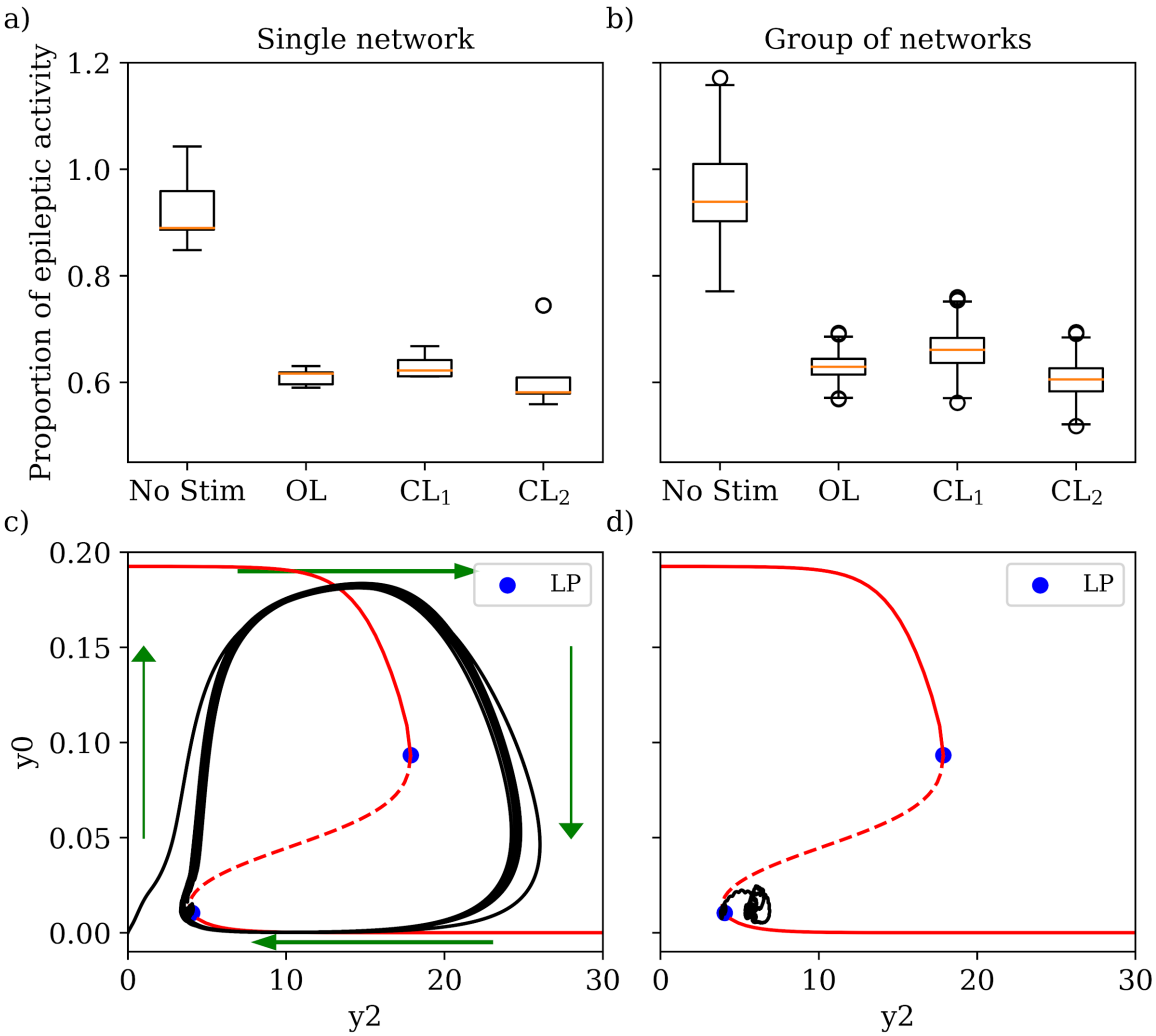

Figure 5. a,b) Boxes showing normalized *AEDI* values (proportion of epileptic activity) while stimulating randomly (OL) or at epileptic spike onsets (CL_1), or 0.25 s before their onset (CL_2). c,d) the projection y_3-nullcline and trajectories of the Jansen-Rit NMM (eq.1) in the plane (y_2, y_0), while synaptic gains were fixed to generate spiking activity, in the absence and presence of a charge-balanced biphasic pulse stimulation (amp=3 mV, freq=90 Hz) applied one second before spiking onset, respectively. In (b) both connectivity coefficients and noise are modified (Group of networks), unlike (a) where only the noise is modified (Single network). The boxes mean values from left to right are [(a: {0.92, 0.61, 0.63, 0.60}), (b: {0.94, 0.63, 0.66, 0.60})]. Continuous and dashed parts of the red curve represent stable and unstable branches of the y_3-nullcline, respectively, where the blue points represent the folds of the curve. The green arrows represent the flow direction.

In addition to emphasizing the effectiveness of multi-site stimulation, Figure 5 enables the comparison between closed- and open-loop stimulation protocols, and illustrates the impact of stimulation timing. Figures 5a) and 5b) present the proportion of epileptic activity in the absence of stimulation (NoStim), after applying a stimulation regardless of oscillation onset (OL), at oscillation onset (CL_1), and onset (CL_2). This

proportion is defined as the ratio of the product of the number of interictal discharges and their duration divided by the signal's duration.

Using a charge-balanced biphasic stimulation of amplitude 3 mV and a frequency of 90 Hz upon all network NMMs, and for a total of 500 simulations in the case of one or group of networks (single or different individuals) (as the connectivity coefficients are fixed or not), we found that OL stimulation reduced the proportion of epileptic activity by 30 % and provided similar results as compared to (CL_1) stimulation. However, $(CL_2)$was more efficient than the other two forms of neuromodulation with this difference being due to the timing of the stimulation with respect to the onset of epileptiform activity. In order to illustrate this difference, we projected the y_3-nullcline and the system response to stimulation (black curves) on the (y_2, y_0)-plane in panels c and d of Figure 5. The green arrows in panel 5c show the flow direction. By taking the right hand side of the Jansen and Rit NMM to 0, we obtain:

$$
\begin{aligned}
&y_3 = y_4 = y_5 = 0\\
&y_0 = (A/a) \times Sig(y_1 - y_2)\\
&y_1 = (A/a) \times \{p + C_2 Sig(C_1 y_0)\}\\
&y_2 = (B/b) \times C_4 Sig(C_3 y_0)
\end{aligned}
$$

The y_3-nullcline is given by the following function depending on y_0 and driven from the system above,

$$
y_2 = func(y_0) = (A/a) \times \{p + C_2 Sig(C_1\, y_0)\} - Sig^{-1}((a/A) y_0),\ y_0 \in]0, Ae_0/a[\qquad \textbf{(3)}
$$

Notice that the function (3) yields a hysteresis curve, along which the large amplitude oscillations take place by jumping between the upper and lower branches and passing close to the fold points (Iasemidis et al., 2003; Prasad et al., 2005; Sackellares et al., 2000). A closed-loop stimulation algorithm based on oscillations detection would be inefficient to prevent the system from oscillating, since such stimulation would be applied when the flow takes off after passing close to the left hand side fold point. In order to prevent large amplitude oscillations and maintain background activity, the stimulation should be applied before the system reaches the left hand side fold point (Figure 5d). Otherwise, once a spike was triggered, it was not possible to stop it until it approaches this point.

3.4 Resonance phenomena

We studied the effects of stimulation frequency while a single unconnected NMM was generating background activity. The average excitatory and inhibitory synaptic gains were fixed to 6 and 7 mV, respectively. All other model parameters were equal to the values presented in Table 1.

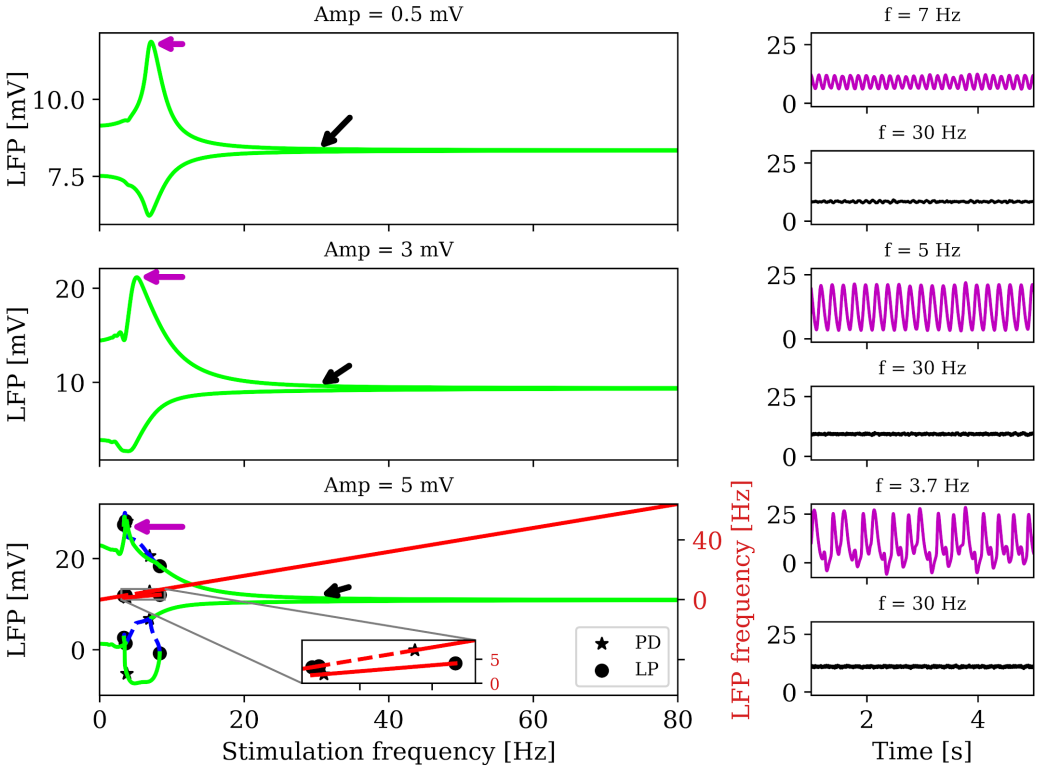

Figure 6. (*Left panels*) LFP amplitude and frequency as a function of stimulation frequency. (*Right panels)* Corresponding resonant and nonresonant time series. The same sinusoidal stimulation was added to the postsynaptic potential entering all model subpopulations, $(k_e, k_i) = (1, 1)$. Stable and unstable limit cycles are represented by solid green and dashed blue lines, while their frequencies are represented by solid and dashed red lines, respectively. The stars and circles denote period-doublings (PD) and limit points (LP), respectively.

Figure 6 shows LFP amplitude as a function of the stimulation frequency per stimulation amplitude. Depending on the stimulation amplitude, the system had a different resonance frequency for which high-amplitude oscillations appear. By increasing the stimulation amplitude, the model had a smaller resonance frequency where it generated oscillations of large amplitude. For a stimulation amplitude equal to 0.5 mV *(upper panel)*, the resonance frequency was 7 Hz. However, by increasing the stimulation amplitude to 5 mV (lower panel), the resonance frequency decreased to 3.5 Hz and bifurcation points started to appear unlike upper and middle panels.

For *f = 6.9 Hz,* a period doubling bifurcation was detected, and the respective limit cycle lost stability with half the frequency of the stable cycle. Then, another period doubling bifurcation point was detected for *f = 3.58 Hz* previoused by a limit point for *f = 3.35 Hz.* This PD point led to another change in stability and a doubling of the frequency of limit cycles. For $f \in]3.35, 8.3[$ *Hz*, the system was attracted by stable and unstable attractors and the LFP frequency domain included other frequencies in addition to the stimulation frequency.

4 Discussion and concluding remarks

Several computational, experimental and clinicals studies have been conducted to investigate neuromodulation effects and parameters to control epileptiform activity in epileptogenic networks. The prospective of multi-site stimulation in epilepsy is in part motivated by reported effects of multi-site stimulation in humans, for example in working memory enhancement (Alagapan et al., 2019). In this study, we developed a computational model of an epileptogenic neuronal network and studied the impact of multi-site stimulation on connected neuronal populations generating interictal discharges; an activity recognized as an electrophysiological marker of epileptogenic neuronal systems (Wendling et al., 2012). Let us mention that, in our model, no mechanism was included to account for the potential lasting effects of the stimulation. Therefore, the effects quantified and presented in this study account for when the stimulation is applied, but no lasting effects are presented from the nature of the developed model that only describes acute effects of the stimulation. Our results confirmed the effectiveness of multi-site stimulation in reducing the frequency of epileptic discharges, and have shown that it is possible to guide the choice of stimulation targets based on a graph theory metric. The efficiency of multi-site stimulation is related to the circuit structure and connectivity: the afferents received by a neuronal region belonging to a network can indeed lead to the excitation of a neuronal subpopulation responsible for generating seizures (Burns et al., 2014; Martinet et al., 2017). We also presented a method for selecting and limiting the number of target populations. These chosen connectivity hubs are characterized by a high output functional connectivity, and stimulating those populations strongly impacts network dynamics, as opposed to other locations. This result is related to the studied neuronal network and may not always be the case when studying a different one. Past and most recent studies show that the epileptogenic focus was associated with a population with the maximum information inflow interictally, possibly to keep the focus under control (Krishnan et al., 2015; Narasimhan et al., 2020; Vlachos et al., 2017). Moreover, it is worth mentioning that multi-site stimulation of a few populations was identified as optimal, and outperformed stimulation of the entire network or of a single region.

We have shown that closed-loop stimulation based on the detection of low-frequency epileptiform activity is able to suppress interictal discharges. However, the difference as compared to open-loop stimulation while the system is in an epileptogenic state was minimal. Despite this similar performance, a closed-loop paradigm should be preferred since stimulation is only delivered if and when needed, minimizing interaction with brain tissue. Noteworthy, both open-loop and closed-loop approaches have been shown to effectively reduce seizure frequency. Several studies emphasize the effectiveness of closed loop stimulation compared to open loop stimulation in aborting seizures (Salam et al., 2016; Skarpaas et al., 2019). However, there exist other studies claiming the opposite (Vassileva et al., 2018). Therefore, there is still no consensus on this question and further investigations are still needed to determine which approach is the best, or if a combination of both should be considered

depending on the objective. In this study, in addition to the frequent presence of epileptic activities in the generated signals, stimulation using an open-loop approach was delivered the same number of times as for closed loop stimulation and for a fixed duration. In clinical cases, open- and closed-loop stimulation are applied differently (Bigelow and Kouzani, 2019): open-loop stimulations deliver stimulations repetitively for a pre-set duration and may not necessarily be applied during an ictal period, while closed-loop stimulations are applied once seizure onset is detected. Therefore, in our specific case, the results from the “closed-loop” scheme of abatement of epileptic spikes we applied showed only a marginal advantage over the “open-loop” scheme we employed.

Furthermore, our study provides new insights on the role that GABAergic inhibitory neurons play in the activity regulation of excitatory neurons (Ingram et al., 2019; Komarov et al., 2019). We assume that the capability to selectively activate specific neuronal types will greatly enhance the efficiency of brain stimulation by reducing termination time and minimizing seizure spread. We propose that this prediction of the model could be tested experimentally using optogenetics, which enables the selective activation of specific neuronal populations. In addition, we identified a resonant frequency to avoid in brain stimulation protocols for epilepsy, since stimulation delivered at this frequency can enhance the generation of epileptiform patterns and favor the generation of high-amplitude oscillations, which is amplified by network effects. Therefore, in order to replace epileptiform activity by a more “physiological” activity, it would be appropriate to avoid using such resonant frequencies as stimulation frequencies.

In terms of limitations, avenues for improvement would constitute adoption of more realistic models, such as the Wendling neural mass model (Wendling et al., 2002) comprising somatic-projecting interneurons of faster synaptic kinetics, and having the ability to generate more diverse activities (e.g., fast onset activity) and then taking into account additional outputs resulting from neuronal interactions. In the presence of these fast components, the circuit structure could be reconsidered by including feedforward inhibition to the feedforward excitation adopted here (Chen et al., 2017; Womelsdorf et al., 2014). Moreover, the impact of stimulation on an ongoing seizure instead of interictal spikes presented in this study could be investigated. Noteworthy, previous in-silico seizure-control investigations, assuming that the pathological feedback in brain circuitry is responsible for seizure generation, have been conducted and continuous closed-loop stimulation based on internal feedback were designed to desynchronize the epileptic activity (Chakravarthy et al., 2009b, 2009a, 2007; Tsakalis et al., 2006; Tsakalis and Iasemidis, 2006). Finally, the biophysics layer of the model describing the impact of the electrical stimulation onto neuronal types could be improved by using experimental data linking the amplitude of *in situ* electric fields with the corresponding depolarization at the level of neuron membranes (Bikson et al., 2004).

Acknowledgments

This work is supported by the National Institutes of Health (NIH), R01 grant (R01NS092760-01A1).

References

Alagapan, S., Riddle, J., Huang, W.A., Hadar, E., Shin, H.W., Fröhlich, F., 2019. Network-Targeted, Multi-site Direct Cortical Stimulation Enhances Working Memory by Modulating Phase Lag of Low-Frequency Oscillations. Cell Reports 29, 2590-2598.e4. https://doi.org/10.1016/j.celrep.2019.10.072

Badawy, R. a. B., Freestone, D.R., Lai, A., Cook, M.J., 2012. Epilepsy: Ever-changing states of cortical excitability. Neuroscience 222, 89–99. https://doi.org/10.1016/j.neuroscience.2012.07.015

Bigelow, M.D., Kouzani, A.Z., 2019. Neural stimulation systems for the control of refractory epilepsy: a review. J Neuroeng Rehabil 16. https://doi.org/10.1186/s12984-019-0605-x

Bikson, M., Inoue, M., Akiyama, H., Deans, J.K., Fox, J.E., Miyakawa, H., Jefferys, J.G.R., 2004. Effects of uniform extracellular DC electric fields on excitability in rat hippocampal slices in vitro. The Journal of Physiology 557, 175–190. https://doi.org/10.1113/jphysiol.2003.055772

Burns, S.P., Santaniello, S., Yaffe, R.B., Jouny, C.C., Crone, N.E., Bergey, G.K., Anderson, W.S., Sarma, S.V., 2014. Network dynamics of the brain and influence of the epileptic seizure onset zone. Proc. Natl. Acad. Sci. U.S.A. 111, E5321-5330. https://doi.org/10.1073/pnas.1401752111

Chakravarthy, N., Sabesan, S., Iasemidis, L., Tsakalis, K., 2007. Controlling synchronization in a neuron-level population model. Int J Neural Syst 17, 123–138. https://doi.org/10.1142/S0129065707000993

Chakravarthy, N., Sabesan, S., Tsakalis, K., Iasemidis, L., 2009a. Controlling epileptic seizures in a neural mass model. J Comb Optim 17, 98–116. https://doi.org/10.1007/s10878-008-9182-9

Chakravarthy, N., Tsakalis, K., Sabesan, S., Iasemidis, L., 2009b. Homeostasis of brain dynamics in epilepsy: a feedback control systems perspective of seizures. Ann Biomed Eng 37, 565–585. https://doi.org/10.1007/s10439-008-9625-6

Chen, G., Zhang, Y., Li, X., Zhao, X., Ye, Q., Lin, Y., Tao, H.W., Rasch, M.J., Zhang, X., 2017. Distinct Inhibitory Circuits Orchestrate Cortical beta and gamma Band Oscillations. Neuron 96, 1403-1418.e6. https://doi.org/10.1016/j.neuron.2017.11.033

Freeman, W.J., 1975. Mass Action in the Nervous System: Examination of the Neurophysiological Basis of Adaptive Behavior Through the EEG. Academic Press.

Good, L.B., Sabesan, S., Marsh, S.T., Tsakalis, K., Treiman, D., Iasemidis, L., 2009. Control of synchronization of brain dynamics leads to control of epileptic seizures in rodents. Int J Neural Syst 19, 173–196. https://doi.org/10.1142/S0129065709001951

Hoang, K.B., Cassar, I.R., Grill, W.M., Turner, D.A., 2017. Biomarkers and Stimulation Algorithms for Adaptive Brain Stimulation. Front Neurosci 11. https://doi.org/10.3389/fnins.2017.00564

Hodgkin, A.L., Huxley, A.F., 1952. A quantitative description of membrane current and its application to conduction and excitation in nerve. J Physiol 117, 500–544.

Iasemidis, L., Prasad, A., Sackellares, J.C., Pardalos, P., Shiau, D., 2003. On the prediction of seizures, hysteresis and resetting of the epileptic brain: insights from models of coupled chaotic oscillators. Order and chaos 8 283–305.

Ingram, T.G.J., King, J.L., Crowder, N.A., 2019. Divisive Inhibition Prevails During Simultaneous Optogenetic Activation of All Interneuron Subtypes in Mouse Primary Visual Cortex. Front Neural Circuits 13. https://doi.org/10.3389/fncir.2019.00040

Jansen, B.H., Rit, V.G., 1995. Electroencephalogram and visual evoked potential generation

in a mathematical model of coupled cortical columns. Biol. Cybern. 73, 357–366. https://doi.org/10.1007/BF00199471
Katchanov, J., Birbeck, G.L., 2012. Epilepsy care guidelines for low- and middle- income countries: From WHO mental health GAP to national programs. BMC Med 10, 107. https://doi.org/10.1186/1741-7015-10-107
Kobau, R., Zahran, H., Thurman, D.J., Zack, M.M., Henry, T.R., Schachter, S.C., Price, P.H., Centers for Disease Control and Prevention (CDC), 2008. Epilepsy surveillance among adults--19 States, Behavioral Risk Factor Surveillance System, 2005. MMWR Surveill Summ 57, 1–20.
Komarov, M., Malerba, P., Golden, R., Nunez, P., Halgren, E., Bazhenov, M., 2019. Selective recruitment of cortical neurons by electrical stimulation. PLOS Computational Biology 15, e1007277. https://doi.org/10.1371/journal.pcbi.1007277
Krishnan, B., Vlachos, I., Wang, Z.I., Mosher, J., Najm, I., Burgess, R., Iasemidis, L., Alexopoulos, A.V., 2015. Epileptic focus localization based on resting state interictal MEG recordings is feasible irrespective of the presence or absence of spikes. Clin Neurophysiol 126, 667–674. https://doi.org/10.1016/j.clinph.2014.07.014
Kwan, P., Brodie, M.J., 2000. Early identification of refractory epilepsy. N. Engl. J. Med. 342, 314–319. https://doi.org/10.1056/NEJM200002033420503
Lee, K., Khoo, H.M., Lina, J.-M., Dubeau, F., Gotman, J., Grova, C., 2018. Disruption, emergence and lateralization of brain network hubs in mesial temporal lobe epilepsy. Neuroimage Clin 20, 71–84. https://doi.org/10.1016/j.nicl.2018.06.029
Lévesque, M., Salami, P., Shiri, Z., Avoli, M., 2018. Interictal oscillations and focal epileptic disorders. European Journal of Neuroscience 48, 2915–2927. https://doi.org/10.1111/ejn.13628
Lopes da Silva, F., Pijn, J.P., Boeijinga, P., 1989. Interdependence of EEG signals: linear vs. nonlinear associations and the significance of time delays and phase shifts. Brain Topogr 2, 9–18. https://doi.org/10.1007/BF01128839
Martinet, L.-E., Fiddyment, G., Madsen, J.R., Eskandar, E.N., Truccolo, W., Eden, U.T., Cash, S.S., Kramer, M.A., 2017. Human seizures couple across spatial scales through travelling wave dynamics. Nature Communications 8, 14896. https://doi.org/10.1038/ncomms14896
Maruyama, G., 1955. Continuous Markov processes and stochastic equations. Rend. Circ. Mat. Palermo 4, 48. https://doi.org/10.1007/BF02846028
Narasimhan, S., Kundassery, K.B., Gupta, K., Johnson, G.W., Wills, K.E., Goodale, S.E., Haas, K., Rolston, J.D., Naftel, R.P., Morgan, V.L., Dawant, B.M., González, H.F.J., Englot, D.J., 2020. Seizure-onset regions demonstrate high inward directed connectivity during resting-state: An SEEG study in focal epilepsy. Epilepsia. https://doi.org/10.1111/epi.16686
Ngugi, A.K., Kariuki, S.M., Bottomley, C., Kleinschmidt, I., Sander, J.W., Newton, C.R., 2011. Incidence of epilepsy: a systematic review and meta-analysis. Neurology 77, 1005–1012. https://doi.org/10.1212/WNL.0b013e31822cfc90
Pijn, J.P., Lopes da Silva, F., 1993. Propagation of Electrical Activity: Nonlinear Associations and Time Delays between EEG Signals, in: Zschocke, S., Speckmann, E.-J. (Eds.), Basic Mechanisms of the EEG, Brain Dynamics. Birkhäuser, Boston, MA, pp. 41–61. https://doi.org/10.1007/978-1-4612-0341-4_4
Prasad, A., Iasemidis, L.D., Sabesan, S., Tsakalis, K., 2005. Dynamical hysteresis and spatial synchronization in coupled non-identical chaotic oscillators. Pramana - J Phys 64, 513–523. https://doi.org/10.1007/BF02706199
Radman, T., Ramos, R.L., Brumberg, J.C., Bikson, M., 2009. Role of cortical cell type and morphology in subthreshold and suprathreshold uniform electric field stimulation in vitro. Brain Stimulation 2, 215-228.e3. https://doi.org/10.1016/j.brs.2009.03.007
Roehri, N., Pizzo, F., Lagarde, S., Lambert, I., Nica, A., McGonigal, A., Giusiano, B., Bartolomei, F., Bénar, C.-G., 2018. High-frequency oscillations are not better biomarkers of epileptogenic tissues than spikes. Annals of Neurology 83, 84–97. https://doi.org/10.1002/ana.25124

Sackellares, J.C., Iasemidis, L.D., Shiau, D.-S., Gilmore, R.L., Roper, S.N., 2000. Epilepsy ? when chaos fails, in: Chaos in Brain? WORLD SCIENTIFIC, pp. 112–133. https://doi.org/10.1142/9789812793782_0010
Salam, M.T., Perez Velazquez, J.L., Genov, R., 2016. Seizure Suppression Efficacy of Closed-Loop Versus Open-Loop Deep Brain Stimulation in a Rodent Model of Epilepsy. IEEE Trans Neural Syst Rehabil Eng 24, 710–719. https://doi.org/10.1109/TNSRE.2015.2498973
Sankaraneni, R., Lachhwani, D., 2015. Antiepileptic drugs--a review. Pediatr Ann 44, e36-42. https://doi.org/10.3928/00904481-20150203-10
Skarpaas, T.L., Jarosiewicz, B., Morrell, M.J., 2019. Brain-responsive neurostimulation for epilepsy (RNS® System). Epilepsy Res. 153, 68–70. https://doi.org/10.1016/j.eplepsyres.2019.02.003
Sobayo, T., Mogul, D.J., 2016. Should stimulation parameters be individualized to stop seizures: Evidence in support of this approach. Epilepsia 57, 131–140. https://doi.org/10.1111/epi.13259
Spiegler, A., Jirsa, V., 2013. Systematic approximations of neural fields through networks of neural masses in the virtual brain. Neuroimage 83, 704–725. https://doi.org/10.1016/j.neuroimage.2013.06.018
Suffczynski, P., Kalitzin, S., da Silva, F.L., Parra, J., Velis, D., Wendling, F., 2008. Active paradigms of seizure anticipation: computer model evidence for necessity of stimulation. Phys Rev E Stat Nonlin Soft Matter Phys 78, 051917. https://doi.org/10.1103/PhysRevE.78.051917
Tsakalis, K., Chakravarthy, N., Sabesan, Sh., Iasemidis, L.D., Pardalos, P.M., 2006. A feedback control systems view of epileptic seizures. Cybern Syst Anal 42, 483–495. https://doi.org/10.1007/s10559-006-0087-2
Tsakalis, K., Iasemidis, L., 2006. Control aspects of a theoretical model for epileptic seizures. Int. J. Bifurcation Chaos 16, 2013–2027. https://doi.org/10.1142/S0218127406015866
Upton, A.R., Cooper, I.S., 1976. Some neurophysiological effects of cerebellar stimulation in man. Can J Neurol Sci 3, 237–254.
Vassileva, A., van Blooijs, D., Leijten, F., Huiskamp, G., 2018. Neocortical electrical stimulation for epilepsy: Closed-loop versus open-loop. Epilepsy Research 141, 95–101. https://doi.org/10.1016/j.eplepsyres.2018.02.010
Vlachos, I., Krishnan, B., Treiman, D.M., Tsakalis, K., Kugiumtzis, D., Iasemidis, L.D., 2017. The Concept of Effective Inflow: Application to Interictal Localization of the Epileptogenic Focus From iEEG. IEEE Trans Biomed Eng 64, 2241–2252. https://doi.org/10.1109/TBME.2016.2633200
Wendling, F., Bartolomei, F., Bellanger, J.J., Chauvel, P., 2002. Epileptic fast activity can be explained by a model of impaired GABAergic dendritic inhibition. European Journal of Neuroscience 15, 1499–1508. https://doi.org/10.1046/j.1460-9568.2002.01985.x
Wendling, F., Bartolomei, F., Mina, F., Huneau, C., Benquet, P., 2012. Interictal spikes, fast ripples and seizures in partial epilepsies – combining multi-level computational models with experimental data. European Journal of Neuroscience 36, 2164–2177. https://doi.org/10.1111/j.1460-9568.2012.08039.x
Wendling, F., Bellanger, J.J., Bartolomei, F., Chauvel, P., 2000. Relevance of nonlinear lumped-parameter models in the analysis of depth-EEG epileptic signals. Biol Cybern 83, 367–378. https://doi.org/10.1007/s004220000160
Wendling, F., Benquet, P., Bartolomei, F., Jirsa, V., 2016. Computational models of epileptiform activity. Journal of Neuroscience Methods, Methods and Models in Epilepsy Research 260, 233–251. https://doi.org/10.1016/j.jneumeth.2015.03.027
Womelsdorf, T., Valiante, T.A., Sahin, N.T., Miller, K.J., Tiesinga, P., 2014. Dynamic circuit motifs underlying rhythmic gain control, gating and integration. Nature Neuroscience 17, 1031–1039. https://doi.org/10.1038/nn.3764
Youssofzadeh, V., Agler, W., Tenney, J.R., Kadis, D.S., 2018. Whole-brain MEG connectivity-based analyses reveals critical hubs in childhood absence epilepsy. Epilepsy Res. 145, 102–109. https://doi.org/10.1016/j.eplepsyres.2018.06.001